2021

Vapor stem bubbles dominate heat transfer enhancement in extremely confined boiling

A. A. Alsaati

D. M. Warsinger

J. A. Weibel

A. M. Marconnet

Vapor Stem Bubbles Dominate Heat Transfer Enhancement in Extremely Confined Boiling

A. A. Alsaati, D. M. Warsinger, J. A. Weibel, A. M. Marconnet*

School of Mechanical Engineering, Purdue University, West Lafayette, Indiana, 47907 United States

Highlights

- Investigation sheds light on the fundamental mechanisms of boiling in extremely confined gaps.
- Small residual pockets of vapor, termed 'stem bubbles' herein, remain on the boiling surface.
- Stem bubbles suppress nucleation and reduce surface superheat compared to nucleate boiling.
- A confinement gap spacing threshold is proposed to identify the stem bubble boiling regime.

*Corresponding Author

E-mail Address: marconnet@purdue.edu (A. M. Marconnet)

Abstract

Boiling has long been sought as the heat dissipation mechanism for a wide variety of compact thermal management applications owing to low-resistance heat transport, high heat flux limits, and surface isothermalization. This work aims to elucidate the thermofluidic transport mechanisms of boiling in extremely confined gaps through experimental measure of the temporal evolution of heat fluxes and surface temperatures during deionized water boiling, as well as high-speed visualization of bubble formation. The flow visualizations reveal small residual pockets of vapor, termed 'stem bubbles' herein, that remain on the boiling surface through a pinch-off process vapor escapes through the edges of the confined heated region. These stem bubbles act as seeds for vapor growth in the next phase of the boiling process and dictate the boiling performance for extremely confined boiling as defined based on a dimensionless ratio of the gap spacing to capillary length ($Bo \leq 0.35$ - 0.5). This conclusion is supported by the enhanced thermal response of the surface compared to nucleate boiling. Because activation of nucleation sites is not required for stem bubble boiling, phase change occurs at a reduced surface superheat at a given heat flux compared to nucleate boiling. Criteria for the dimensionless confinement gap spacing are identified to harness this improved heat transfer rate of the stem bubble boiling regime. This new understanding of boiling in extremely confined gaps offers a new direction to design compact two-phase thermal management solutions through using the unique enhancements provided by the vapor stem bubble boiling regime.

Keywords

Confined boiling; liquid-vapor interface; thermal management; two-phase heat transfer; stem bubble.

Nomenclature

Bo	Bond Number, $\frac{S}{L_c}$ (-)
D	Boiling Surface Diameter (m)
d	Vapor Bubble Diameter (m)
D_c	Confinement wall Diameter (m)
d_d	Vapor Bubble Departure Diameter (m)
g	Gravitational Acceleration (m/s^2)
h_∞	Unconfined Heat Transfer Coefficient (W/m^2K)
h_{con}	Confined Heat Transfer Coefficient (W/m^2K)
h_{lv}	Heat of Vaporization (J/kg)
Ja	Jackob Number, $\frac{\rho_l c_{pl}(T_{\inf}-T_{sat})}{\rho_v h_{lv}}$ (-)
k_l	Liquid Thermal Conductivity (W/mK)
L_c	Capillary Length, $\sqrt{\frac{\sigma}{g(\rho_f-\rho_v}}$ (-)
Pr	Prandtl Number, $\frac{c_{pl}\mu}{k}$ (-)
q''	Heat Flux (W/m^2)
q''_i	Incipience Heat Flux (W/m^2)
R	Vapor Bubble Radius (m)
S	Confinement Gap Size (m)
t	Time (s)

t_d Vapor Bubble Departure Time (s)

T_i Incipience Surface Temperature (K)

T_{sat} Saturation Temperature (K)

T_W Wall or Boiling Surface Temperature (K)

Greek Symbols

Γ Non-dimensional Diameter of Bubbles, $\frac{d}{L_c}$ (-)

ν_{lv} Specific Volume Difference (m^3/kg)

ρ_l Liquid Density (kg/m^3)

ρ_v Vapor Density (kg/m^3)

σ Surface Tension (N/m)

1 Introduction

The performance of various electronic systems including data centers, supercomputers, and power electronics depends on the ability to maintain device temperature below a set limit while dissipating a large amount of waste heat [1, 2, 3, 4, 5, 6, 7]. For many years, air-cooled heat sinks and single-phase liquid cold plates have been relied upon to dissipate the heat generated. However, the trend of electronic component miniaturization has driven up heat fluxes to levels where these traditional methods fail to maintain safe operating temperatures. Thermal management using two-phase cooling schemes holds promise to maintain device temperatures within the allowed limits while dissipating higher heat fluxes owing to the latent heat of the cooling. Decades of research on two-phase thermal management solutions, both passive (*i.e.*, vapor chambers [8], heat pipes [9], and immersion cooling [10]) and active (*i.e.*, flow boiling based heat sinks [11]), have significantly matured these technologies. However, aggressive recent trends of embedded cooling, where the coolant flows within the die or package , in addition to the tendency to heterogeneously integrate multiple electronic devices within a single package, poses significant geometrical limitations on the available space in which two-phase cooling solutions can be implemented, motivating a further investigation into the implications of extreme geometric confinement on vapor generation mechanisms during boiling.

Nucleate boiling is the target regime of operation because of it offers the highest heat transfer coefficient in pool boiling. Improving nucleate boiling performance has motivated numerous enhancement techniques that use surface modifications to extend surface area [12], increase nucleation site density [13], and improve surface wicking [14]. These studies generally characterize the bubble nucleation behavior and performance enhancement in unconfined conditions, that is, from a boiling surface submerged in a large pool such that the vapor formed is not affected by the surrounding geometry. On the other hand, in active flow boiling schemes, the coolant is typically pumped through small channels, such that the vapor forms two-phase regimes that are well-known to be affected by the degree of geometric confinement [15, 16, 17, 18]. In confined flow boiling, vapor bubbles span the entire channel cross section; the highest heat transfer coefficient is achieved in the annular flow regime, where bubble nucleation is suppressed, and the main phase change mechanism is evaporation from a thin liquid film surrounding the vapor core. The current investigation, and following review of the literature, focuses on boiling in confined gaps where there is no active pumping. Despite being entirely passive, this situation shares some traits of confined flow boiling in that the volumetric expansion of the fluid during phase change in extremely confined spaces induces a significant local fluid flow where the vapor bubbles are highly confined by the surrounding geometry. Therefore, confined boiling is of interest as a means to passively achieve enhanced heat transfer coefficients beyond unconfined nucleate boiling.

Characteristics of two-phase heat dissipation in confined spaces are different compared to boiling from large surfaces in an unconfined pool. Confinement of the fluid affects the two-phase interface dynamics which affects the flow pattern, wetting dynamics, and, moreover, heat transfer rate. In one of the earliest investigations into confined boiling, Katto and Yokoya [19] found that confined boiling reduces the critical heat flux (CHF) and improves the average heat transfer coefficient compared to unconfined boiling. In particular, boiling of deionized water at atmospheric pressure is sensitive to the confinement gap space for gaps smaller than 2 mm. At gaps of 2 mm and above, the heat transfer characteristics were similar to unconfined pool boiling [20]. Later investigations observed that, in addition to the confinement gap spacing, the area of confined boiling surface impacts the heat transfer characteristics as well. Specifically, the heat transfer coefficient and critical heat flux both reduced when the diameter of confined boiling surface was increased [21]. Further, confined boiling is less sensitive to heater orientation, microgravity, and surface roughness compared to unconfined boiling [22, 23, 24, 25]. Yet, the surface wettability does impact confined boiling, as recent work has shown that using a superhydrophobic confinement wall improved the thermal characteristics of confined boiling [26].

Since Katto and Yokoya [19] observed that the superheat of the boiling surface reduces as the confinement gap becomes smaller than the bubble detachment diameter, scholars have been attributing the enhancement in heat transfer coefficient to the deformation of the vapor bubble by the confinement plate which results in the broadening of its microlayer [19, 20, 21, 22, 23, 24, 25, 26]. This microlayer theory is rooted in the extensive research on unconfined pool boiling for which the high heat transfer rate associated is widely attributed to evaporation of the microlayer of liquid near the three-phase contact line [27, 28]. However, a confinement wall also significantly alters the two-phase interface dynamics, as the bubble must grow within the confined space, and the rewetting of liquid on the boiling surface. Hence, the mechanistic explanation of the enhanced heat transfer rate in confined boiling should consider and encompass the effect of confinement on the complete cycle of vapor bubble growth, departure from the gap, and surface rewetting.

Many experimental studies have provided insight into factors that affect confined boiling enhancement and cannot be attributed to the microlayer enhancements theory. Specifically, past works showed that the heat flux, fluid properties (viz., viscosity), surface coatings, and the geometrical shape of the confinement periphery impact confined boiling. Stutz *et al.* [29] reported that enhancement in heat transfer with confined boiling deteriorates at high heat flux. Even though the combined fluid properties would result in lowering the bubble departure diameter, Lallemand *et al.* [30] observed higher heat transfer coefficient for mixtures of water/ethylene glycol compared to pure water in confined configurations. It was concluded that the increase of fluid viscosity was advantageous for confined boiling at high heat flux. Additionally, Sarode *et al.* [26] experimentally observed that hydrophobic confining surfaces enhance the heat transfer coefficient compared hydrophilic surfaces. Souza *et al.* [31] evaluated nanocoated boiling surfaces for confined boiling. While the nanocoating reduced the heat transfer coefficient in the unconfined case due the reduction of nucleation sites, it is improved in the confined configuration. Furthermore, the enhancement was found to be sensitive to the geometrical divergence rate of the step from the confinement region to the unconfined fluid pool [32]. All of the above enhancements cannot be explained by the microlayer enhancement theory and indicate that the bubble interface dynamics play a critical role in enhancing heat transfer characteristics in confined boiling. Moreover, confined boiling often exhibits unique periodic spikes in the surface temperature as reported by Kapitz *et al.* [25]. In fact, unlike the relatively consistent bubble generation that occurs in unconfined boiling, in our past work [33], the highest heat transfer coefficient for confined boiling was observed within an intermittent boiling regime (a regime uniquely observed in confined boiling having periods of boiling interspersed with sensible heating that causes periodic spikes in the surface temperature). A deeper understanding of this distinct intermittent boiling regime is required to understand the enhancement mechanisms.

To elucidate the mechanisms that impact confined boiling, this study experimentally evaluates confined boiling across a range of gap spacings through quantification of the boiling curves and high-speed visualization of the bubble dynamics. We observe that small residual regions of vapor left behind when vapor from a bubble escapes through the edges of the confined region, termed 'vapor stem bubbles', provide seeds for subsequent boiling without requiring nucleation of a new vapor bubble to continue the cycle of vapor growth and departure. We propose that these vapor stem bubbles, complementary with the microlayer enhancement of the bubble growth process, are a primary mechanism of heat transfer enhancement in confined boiling, particularly in the intermittent boiling regime. In the following sections, we discuss the experimental setup used to investigate the heat transfer in confined boiling and report the influence of gap spacing on the mechanisms of vapor generation observed. Then, boiling curves for various confined geometries are evaluated to identify the dominant enhancement mechanism of confined boiling.

2 Experimental Methods

The confined boiling apparatus, illustrated in Figure 1, is designed to measure the surface heat flux and superheat for a fixed heated surface diameter, D, and controlled confinement gap spacing, S. A glass window with adjustable vertical positioning creates the confined boiling region above the heated surface. A high-speed camera is used to visualize the two-phase interface dynamics, in order to characterize the mechanisms of the enhancement in heat transfer during confined boiling. The confined boiling apparatus, described in detail below, is significantly modified from its original form used for unconfined boiling experiments, previously described by Hunter *et al.* [34].

The quartz glass double-wall vacuum-insulated chamber holds approximately 500 mL of deionized water (HACH-HQ 40d: 0.37 $\mu S\,cm^{-1}$) within a 75 mm inner diameter. The vacuum insulation minimizes heat losses from the liquid pool. The 25.4 mm-diameter boiling surface is oriented horizontally at the bottom of the boiling chamber. Prior to collecting each boiling curve data set, the boiling surface is polished using 2000 grit emery paper to remove any oxidation. After polishing, the boiling surface has a contact angle of 86.8 °. Throughout the experiments the liquid level

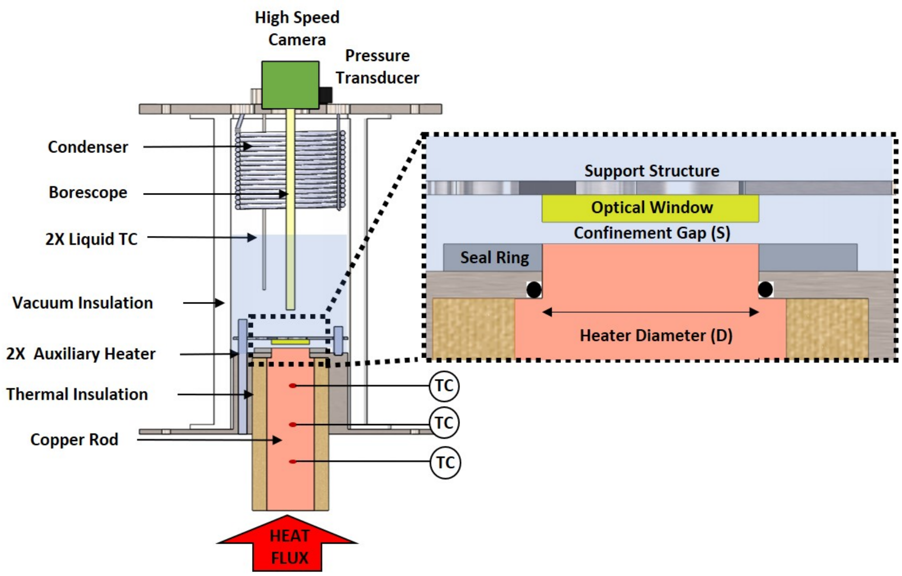

Figure 1: Cross-sectional schematic of the confined boiling experimental apparatus. An electrical heater supplies heat into a copper rod of known thermal conductivity. Three temperature measurements along the rod with embedded thermocouples quantify the heat flux and are extrapolated to estimate the boiling surface temperature. A glass window confines boiling to within the gap of controlled the vertical distance between the boiling surface and the confinement wall, S. A high-speed camera captures the two-phase interface dynamics through a rigid borescope during boiling. Two auxiliary heaters maintain the liquid pool at the saturation temperature. A pressure transducer measures the chamber internal pressure. The exterior of the boiling chamber and the copper rod are well insulated to minimize heat losses.

was maintained about 100 mm above the boiling surface.

A cartridge heater (Watlow Firerod 1039; 12.7 mm diameter, 76.2 mm length; 1000 W) heats the 107.95 mm-long and 31.75 mm-diameter reference copper rod. Adjusting the supplied voltage controls the heat flux into boiling surface. The temperature gradient along the reference rod is measured by three embedded T-type thermocouples (Omega; ±0.3 K). The thermocouples are spaced 6.35 mm apart along the centerline of the reference rod. One-dimensional heat flow is assumed such that the temperature gradient can be linearly correlated to the heat flux at steady state according to Fourier's law. A 18 mm-thick microporous insulation (MICROSIL) covers the perimeter of the reference rod to minimize heat losses. As the reference rod steps down from 31.75 mm diameter to the 25.4 mm diameter boiling surface, the temperature of the boiling surface is linearly extrapolated using a numerically-estimated thermal resistance of the step from the closest thermocouple temperature (12.7 mm below the boiling surface) and the measured heat flux. Minimal spatial temperature inhomogeneities are expected on the boiling surface because of the relativity large copper reference block between the heat source and the boiling surface. The temperature measurements are logged at 1 Hz sampling rate via a data acquisition (DAQ) system (LabJack U6pro) through LabVIEW. The thermocouple cold junction compensation is done using a built-in temperature sensor within the DAQ.

A Viton O-ring seals the reference rod to the boiling chamber. The boiling apparatus body is electrically grounded to reduce measurement noise and prevent charge accumulation. In addition to the main heater, the apparatus is equipped with two additional submerged auxiliary cartridge heaters (Omega HDC19110; 3.2 mm diameter, 88.9 mm length) to maintain the fluid in the reservoir at saturation conditions. To purge non-condensable gases dissolved in the working fluid and trapped within the confinement space, the auxiliary heaters boil the working fluid vigorously for a minimum of 2 h prior to collecting boiling data on saturated water vapor conditions. Throughout the data collection period, the liquid in the reservoir is maintained within 0.3 °C of the saturation temperature by the auxiliary heaters. A condenser coil within the chamber maintains the pressure inside the boiling chamber at 101.8 kPa as monitored using an internal pressure transducer (ASHCROFT, G17MEK15F2VAC/30). An external DC power supply (HP E 3611A) excites the pressure transducer and a DAQ (NI 9219) logs the pressure measurements. A chiller (Thermo Fisher, ARCTIC A 25) circulates 95 °C cooling water through the stainless-steel condenser coil enclosed inside the boiling chamber to condense vapor back to liquid. Two T-type thermocouples (Omega; ±0.3 K) monitor the liquid reservoir temperature.

To study confined boiling, a 6.35 mm-thick circular glass window is suspended above the boiling surface. The confinement window diameter matches the 25.4 mm diameter boiling surface. The confinement window has a static contact angle of 85.0 °. Three spring-loaded set screws level and adjust the confinement gap height, S, with a resolution of 2.2 µm/°. Stainless steel reference shims are used to calibrate the confinement gap spacing. The copper boiling surface protrudes 5.5 mm above the chamber base. To prevent boiling off the sidewalls of this protrusion, a Teflon ring seals (Permatex 81160) and insulates the protruded side walls. The glass confinement window permits top-down optical viewing of the confined boiling region. A high-speed camera (Photron FASTCAM 100K) captures the two-phase interface dynamics at 10,000 frames per second through a rigid borescope (Hawkeye Pro Hardy) submerged in the liquid reservoir. A plasma light source (THORLABS, HPL5345) illuminates the confined test section.

A boiling curve is obtained by measuring the steady state surface superheat as a function of the heat flux supplied to boiling surface. We define steady state as when the temperature measurements vary by less than 0.1 °C/min for 10 min. At steady state, the camera records flow visualization movies of the two-phase interface dynamics. After collecting steady state data at a given heat flux, the power is increased and the system is allowed to reach a new steady state. This process is repeated to obtain the entire boiling curve up to the critical heat flux. This CHF event is observed in the data as a very rapid surface temperature rise and the system is immediately shut down. The highest heat flux reported therefore corresponds to the last steady state data point prior to CHF.

To characterize the influence of confinement, boiling curves are acquired for multiple different confinement gap spacing in separate tests. The confinement gap spacing, S, is varied from 254 µm to 2286 µm. The Bond number, Bo, normalizes the confinement gap spacing by the capillary length, L_c, as:

$$Bo = \frac{S}{L_c} = \frac{S}{\sqrt{\frac{\sigma}{g(\rho_l - \rho_v)}}}, \tag{1}$$

where ρ_l and ρ_v are the density of liquid and vapor respectively, and g is the gravitational acceleration. Boiling is generally considered unconfined when the Bond number is much larger than unity, meaning the size of the vapor bubbles departing the boiling surface are much smaller than the confinement gap spacing. However, the confinement wall interacts with the vapor bubbles when the Bond number is near or below unity. The aforementioned confinement gap spacings are selected to focus on confined boiling behaviors and correspond to a Bond number range from 0.10 (at $S = 254$ µm) to 0.91 (S=2286 µm).

3 Results and Discussion

The confinement gap spacing determines the thermal and the dynamic behavior of confined boiling. This section reports and discuss the visual observations and thermal characteristics as the confinement gap spacing is varied. Two distinct characteristic behaviors are observed with respect to the gap spacing, namely: nucleation-suppressed confined boiling characterized by enhancement of the heat transfer coefficient through vapor stem bubbles; and nucleation-active confined boiling where nucleate boiling predominates by critical heat flux is reduced compared to unconfined conditions.

3.1 Confined Boiling Flow Visualization

Figures 2 and 3 show time series of images from the high-speed flow visualizations that illustrate the confinement gap spacing effect on the two-phase interface dynamics during boiling. A transition in boiling characteristics is observed around some spacing threshold, below which nucleation is suppressed (Figure 2). Vapor bubbles span the gap between the confinement wall and the boiling surface, restricting vapor bubble growth to a two-dimensional plane parallel to the boiling surface. Eventually, the trapped bubble grows and reaches the outer periphery of the confinement zone. The combination of buoyancy and surface tension forces facilitate the extraction of vapor from the confinement zone. Consequently, liquid is replenished from surrounding pool. However, the liquid rewetting rate varies spatially based on the viscous resistance between the two-phase interface and confinement outer periphery. The variable rewetting rate along the two-phase interface results in splitting of the confined vapor bubble as it exits the confinement gap, with only partial escape of the vapor. As illustrated in the supplemental video, no pinning of the interface is observed. This rewetting process leaves a residual vapor 'stem' bubble in the gap from which then next vapor generation cycle stems, and so the process continues in a repeating manner.

In contrast, active nucleation sites are observed for gap spacings larger than the threshold. Vapor is able to completely exhaust from the gap due to the lesser viscous resistance to rewetting, and stem bubbles are not formed. Rather, as shown in Figure 3, isolated spherical vapor bubbles grow from active nucleation sites after vapor departs from the gap. Then, adjacent bubbles formed at different nucleation sites eventually coalesce into single bubbles having lower surface curvature. The change in bubble curvature, and the associated internal pressure forces across the two-phase interface, allowing for an abrupt increase in the growth rate of the coalesced vapor bubble. Due to the complete evacuation of vapor from the confinement gap, the vapor bubbles in following cycles also initiate from vapor embryos at nucleation sites on boiling surface. Note that for nucleation active confined boiling at higher powers,

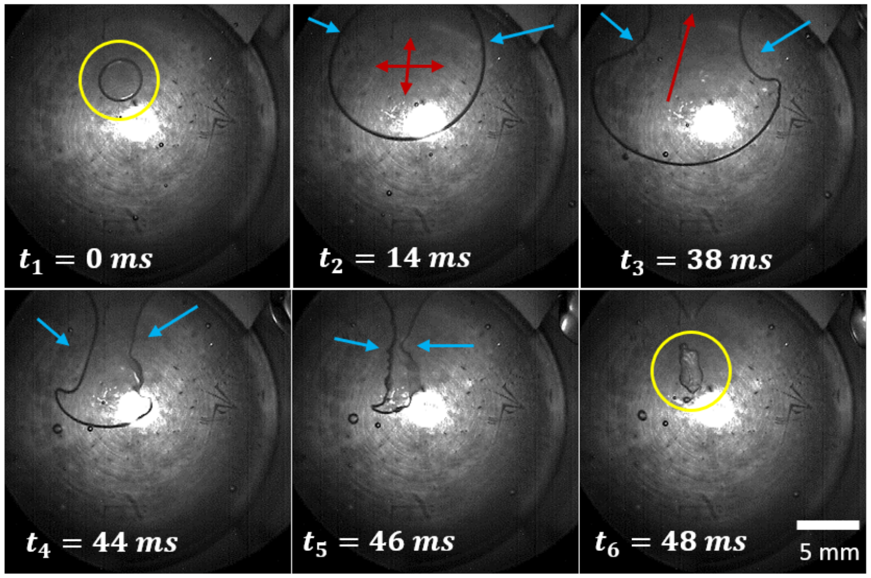

Figure 2: Top view of the boiling surface at several points in time for a nucleation-suppressed confined circular boiling surface ($Bo = 0.30$ with $q" = 10$ W/cm^2). As the vapor expands (red arrows in t_2) and then escapes (red arrow in t_3) confinement, liquid replaces the vapor volume within the confined region (blue arrows in t_4 and t_5). Within the extremely confined boiling region, rewetting occurs at different rates at different positions along the two-phase interface. Viscous resistance slows the rewetting of regions furthers from the confinement edge as shown at time steps t_4 and t_5. As a result, most of the vapor bubble escapes the confined region, but partially leaves behind a stem vapor bubble in the confined space at in time step t_6. This new vapor bubble stems from the vapor left from the preceding vapor bubble and the cycle repeats.

multiple bubbles often form throughout the surface and these cycles happen simultaneously and not necessarily synchronously.

3.2 Effect of Confinement Gap Spacing on Boiling Heat Transfer

Confined boiling curves are measured for five confinement gap spacings from 254 µm to 2286 µm. First, to validate the boiling facility measurements, four repeated unconfined pool boiling curves are measured without suspending the confinement glass

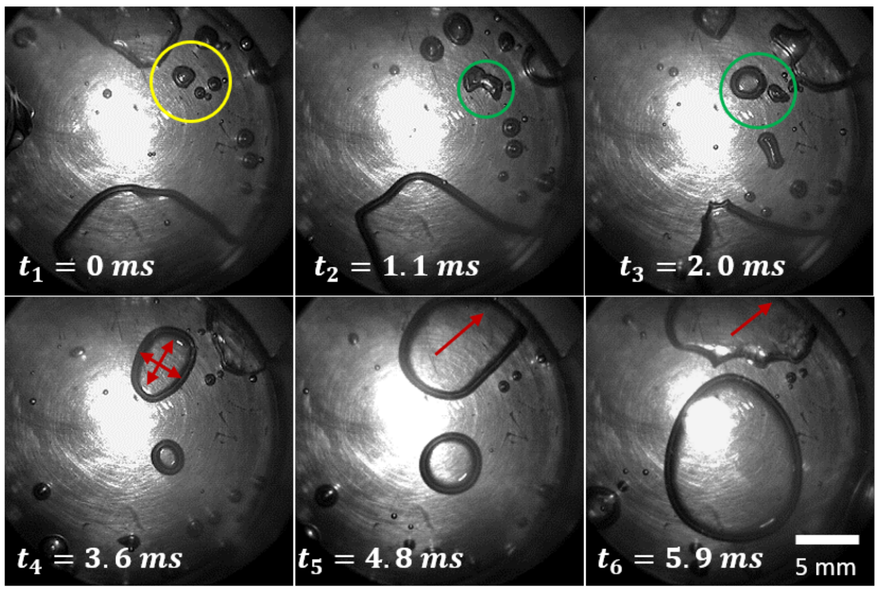

Figure 3: Top view of the boiling surface at several points in time for a nucleation-active confined circular boiling surface ($Bo = 0.63$, $q" = 14$ W/cm^2). Consecutive isolated bubbles forms from an active nucleation site as shown inside the yellow circle at time step t_1. Then, adjacent bubbles formed at different nucleation sites eventually coalesce into single bubbles having lower surface curvature as demonstrated inside the green circles at time steps t_2 and t_3. The change in bubble curvature, and the associated internal pressure forces across the two-phase interface, allow for an abrupt increase in the growth rate of the coalesced vapor bubble (red arrows in time step t_4). The vapor bubble escapes confinement completely when it reaches the confinement edge (red arrows in time steps t_5 and t_6).

above the boiling surface. The measured CHF values of these unconfined pool boiling tests were all within ±6.6% of average measurement (q''_{CHF} = 96.8 W/cm^2). Additionally, the average CHF value is within 12.5% of the theoretical value for finite surfaces [35] of 110.7 W/cm^2.

Boiling curves for varying confinement gap spacing are obtained by measuring the steady state surface superheat as a function of the heat flux supplied to boiling surface. The confined boiling data are compared to the average of the unconfined pool boiling data by plotting the surface superheat (Figure 4) and heat transfer coefficient (Figure 5) as a function of the heat flux.

The transition in the two-phase dynamics characteristics with respect to gap spacing influences the boiling curves during confined boiling. For the case of nucleation-active confined boiling, the minimum incipience superheat criterion for nucleation site activation must be met to initiate and maintain boiling. While surface wettability affects nucleation onset, ultimately, the driving force , surface superheat, must overcome the interface surface tension for a given vapor embryo size for the bubble to grow. Minimum incipience criteria have been developed by Hsu [36, 37] where the vapor embryo is assumed to exist at the mouth of a cavity on the boiling surface and subjected to the bulk liquid temperature gradient as illustrated in Figure 6. Hereafter, the minimum incipient heat flux, q''_i , for a given superheat required for incipience, $T_i - T_{sat}$, is expressed as follow:

$$q''_i = \frac{k_l h_{lv}}{a^* 8 \sigma T_{sat} \nu_{lv}} (T_i - T_{sat})^2, \tag{2}$$

where k_l is the fluid thermal conductivity, h_{lv} is the latent heat of vaporization, σ is the surface tension, ν_{lv} is the difference of specific volume between phases, $T_i - T_{sat}$ is the difference between the minimum incipience surface temperature and saturation temperature, and a^* is a geometrical factor that relates the height of the vapor embryo to the radius of the vapor embryo. Note that we use $a^* = 1.6$ for unconfined boiling while $a^* = 1.0$ for confined boiling. A brief derivation of Equation 2 can be found in the appendix.

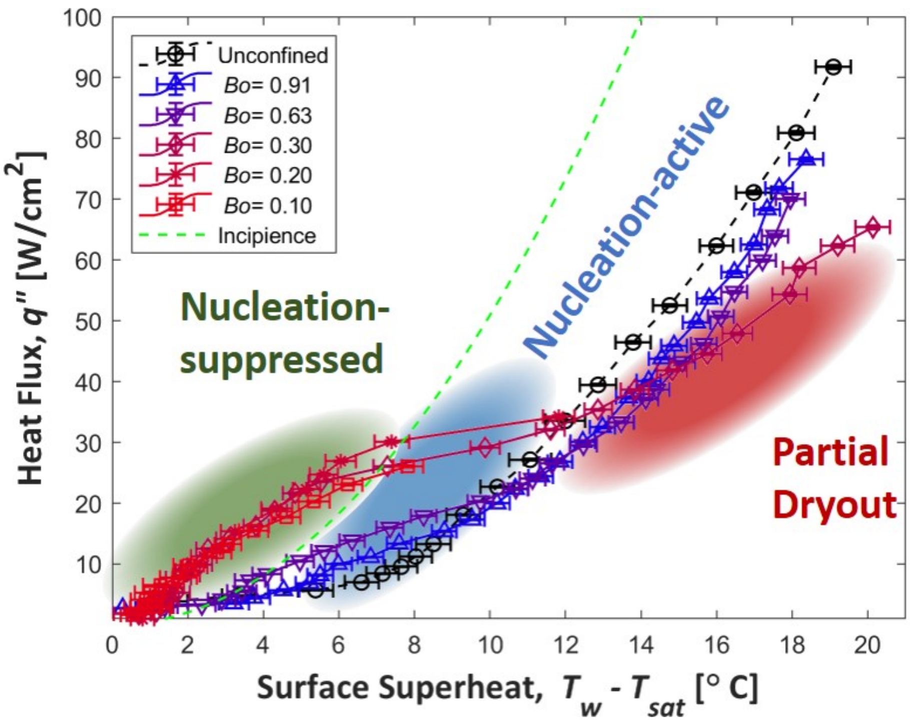

Figure 4: Boiling curves for different non-dimensional confinement gap size ($Bo = S/L_c$). The boiling process spans three distinct characteristics highlighted by different shaded regions. In the *partial dryout* (shaded in red), regions of the boiling surface remain continually covered with vapor due to restriction of liquid replenishing imposed by the confinement wall. As a result, boiling occurs at a higher surface superheat compared to a similar heat flux in the unconfined boiling curve. The blue shaded region is the *nucleation-active* confined boiling region. Nucleation-active confined boiling is limited by the minimum superheat for incipience as expressed in Equation 2 (green dashed line). Enhancements to the heat transfer coefficient are mainly attributed to the larger evaporative microlayer in confined boiling, where active nucleation sites are required to generate new vapor bubble, as demonstrated for nucleation-active confined boiling curves ($Bo = 0.9$ and 0.63). On the other hand, for nucleation-suppressed confined boiling ($Bo = 0.1$, 0.2, and 0.3), vapor generates from the vapor stem bubbles left behind from a previous bubble growth and escape cycle in the *nucleation-suppressed* region (shaded in green). The relatively large radius of stem bubbles compared to vapor embryos allows vapor generation at superheat lower than the minimum superheat required for vapor embryos growth from the boiling surface.

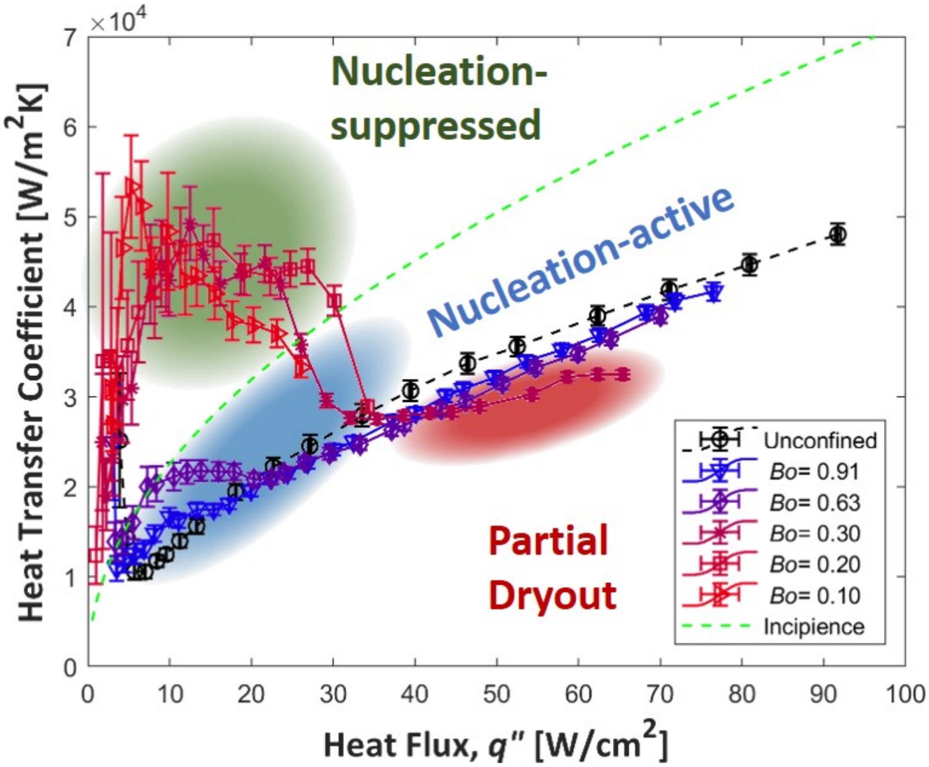

Figure 5: Heat transfer coefficient for different non-dimensional gap sizes ($Bo = S/L_c$) as a function of heat flux. For the unconfined boiling case, the heat transfer coefficient increases with heat flux due to the increase in the active nucleation site density reaching a maximum unconfined heat transfer coefficient at CHF. However, in nucleation-suppressed confined boiling ($Bo = 0.1$, 0.2 and 0.3), the maximum heat transfer coefficient is achieved at the low range of heat flux values due to the stem bubble boiling enhancement mechanism. Similar enhancements are not observed in nucleation-active confined boiling ($Bo = 0.63$ and 0.9), where the main heat transfer coefficient enhancement mechanism is the extension in the area of the evaporative microlayer which is limited to the minimum incipience superheat criterion (dashed green line).

For unconfined boiling, during nucleate boiling, new vapor bubbles grow from the residual vapor embryo left behind the departed bubbles at the nucleation site in a cyclic manner, usually referred to as the ebullition cycle. The residual vapor bubble radii are larger than cavity mouth radius [36], and therefore, boiling can be maintained at active nucleation sites at superheats lower than the incipience criterion for the unconfined configuration. However, nucleation-active confined boiling improvement is limited by the minimum incipient boiling criteria expressed in Equation 2 (nucleate boiling is highlighted in the blue shaded region). In the nucleation-active confined boiling curves ($Bo = 0.63$ and 0.91), at low heat fluxes, the vapor bubbles expand parallel to the boiling surface. This increases the microlayer area underneath the vapor bubble which enhances heat transfer rate at a given surface superheat relative to the unconfined boiling curves. We attribute the microlayer enhancement constraint in nucleation-active confined boiling to hydrodynamic deactivation of nucleation sites. As the confined vapor bubbles grow parallel to boiling surface, the induced flow agitates the protruded region of the residual vapor bubble and reduces its radius to the surface cavity mouth radius as illustrated in Figure 6. As a result, the minimum criteria for incipient boiling is required to maintain nucleation-active confined boiling.

In contrast, in the nucleation-suppressed confined boiling (green-shaded region), vapor stem bubbles are available to sustain phase change without requiring activation or growth of vapor embryo at nucleation sites (as in the nucleation-active confined boiling). Nevertheless, an active nucleation site is needed only to initiate the phase change process in the nucleation-suppressed region resulting in initial temperature overshoot. However, after boiling initiation, an active nucleation site is no longer needed and stem bubbles facilitate thermal enhancements beyond the minimum incipience boiling criterion in nucleation-suppressed confined boiling cases ($Bo = 0.10$, 0.20, and 0.30). On the other hand, once the minimum incipience boiling criterion is met at the higher range of heat flux (Equation 2), simultaneous occurrence of both vapor stem bubbles and nucleate boiling are visually observed as illustrated in the supplemental video. Bubbles nucleate while the liquid rewets the boiling surface,

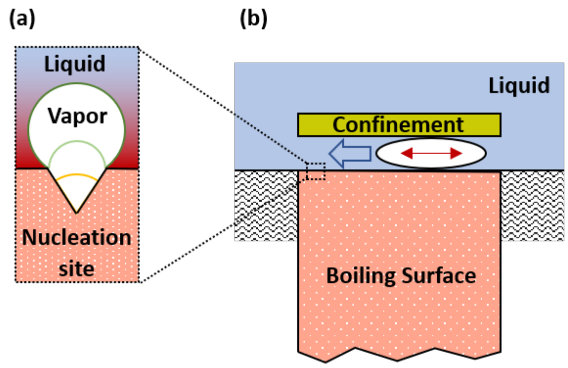

Figure 6: Schematic of (a) bubble growth at a nucleation site and (b) bubble growth within a confined boiling system. As the confined vapor bubble grows parallel to boiling surface (red arrow), the induced flow (blue arrow) agitates the protruded region of the vapor embryos and reduces its radius to the local surface roughness on the boiling surface. As a result, nucleation sites within the confined boiling space are hydrodynamically deactivated and the minimum superheat for nucleation onset is required to maintain boiling within the confined space. Note the color gradient in the left panel illustrates the temperature gradient from the surface temperature (red) to the saturation temperature (blue).

limiting the radial inward penetration of the liquid in the confined gap. As a result, the nucleation-suppressed confined boiling curves abruptly shifts into a partial dryout boiling region where regions of boiling surface remain continually covered in vapor due to the restriction of liquid replenishing imposed by the confinement wall. Consequently, the average boiling surface superheat exceeds the equivalent superheat of an unconfined boiling in a similar heat flux value (red shaded region). This notable shift in surface superheat indicates *that stem bubble boiling is the dominant heat transfer enhancement mechanism leading to an increased heat transfer coefficient in nucleation-suppressed confined boiling configurations.*

3.3 Vapor Stem Bubbles

Figure 7 schematically illustrates the proposed mechanism by which vapor stem bubbles enhance heat transfer in confined boiling configurations. The significant viscous resistance varies the rewetting rate along the two-phase interface in nucleation-suppressed confined boiling which results in splitting of the confined vapor bubble as it exits the confinement gap, with only partial escape of the vapor. The size of residual vapor stem bubble is on the same scale as the confinement gap spacing. Due to the difference in two-phase interface radius, surface tension forces on vapor stem bubbles are weaker compared to vapor embryos in nucleation site. Hence, the vapor stem bubble can begin to grow at surface superheat lower than incipience minimum criterion and without requiring activation of additional nucleation sites on the boiling surface, thereby lowering the overall thermal resistance in nucleation-suppressed confined boiling.

The concept of vapor stem bubbles can potentially explain some of the previous confined boiling experimental observations that cannot be explained by the microlayer theory enhancement alone, as reviewed in the introduction. In boiling regimes with these vapor stem bubbles, interface dynamics and fluid viscosity control the formation of the residual stem bubble. Further, the chaotic nature of boiling has a stochastic effect on forming the residual stem bubble within the confined space. In other words, even for a steady constant operating condition, there is a probability of complete vapor bubble escape for which a stem vapor bubble is not left behind for the next bubble generation cycle. In this case, active nucleation sites are required to reinitiate phase change on boiling surface. Since, these nucleation-site vapor embryos have smaller radius than the vapor stem bubble, the heat will momentarily be dissipated through the sensible heating of local fluid until the minimum superheat required for nucleation site activation is reached. As a result, the high heat transfer coefficient caused by the phase change is briefly not observed. This momentary pause of phase change would result in the distinct intermittent boiling regimes uniquely observed in confined boiling configurations [33].

Vapor stem bubbles are formed during confined boiling only when confinement gap is smaller than a spacing threshold. In order to harness the enhanced thermal performance of this boiling behavior in applications, it is crucial to generally predict

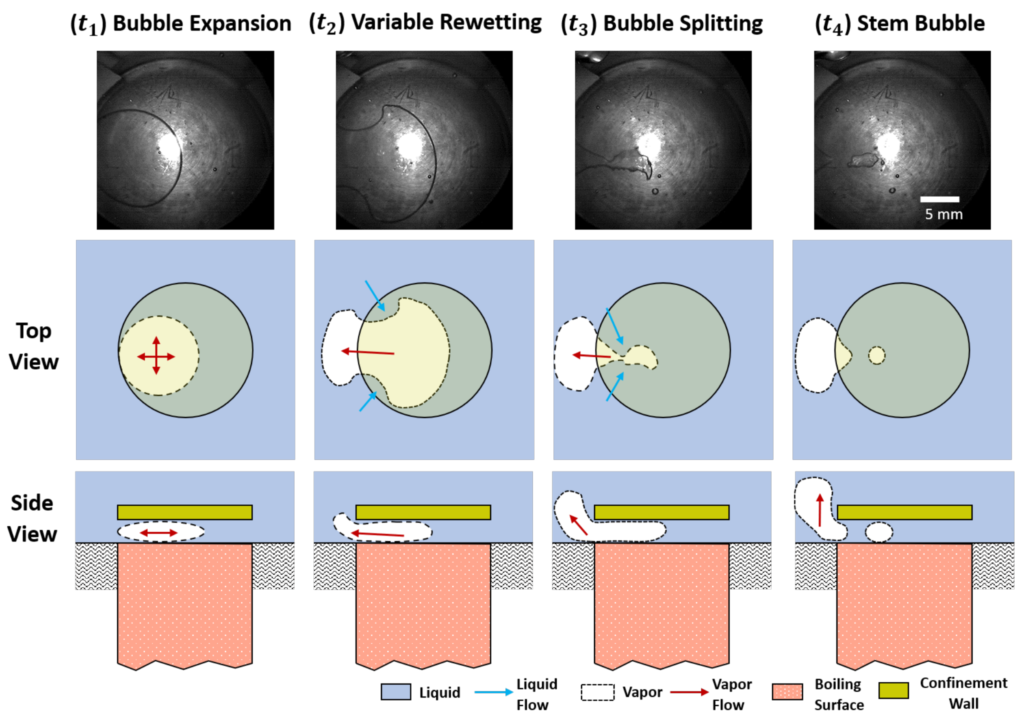

Figure 7: Flow visualizations and complementary schematics of the cycle of bubble growth and escape in nucleation-suppressed confined boiling. The time series demonstrates a life cycle of vapor bubble growing between the boiling surface and the confinement wall. In the first image t_1, confinement limits the bubble to growing only parallel to the boiling surface. After the bubble reaches the edge of the confined zone, it can escape into the liquid pool. Liquid replaces the escaped vapor bubble at variable wetting rates across the two-phase interface, t_2. The red arrows illustrate the vapor outflow of the confinement and the blue arrows illustrate the liquid inflow. Viscous resistance slows the rewetting for regions furthest from confinement edge which results in vapor splitting and partial vapor escape as illustrated in t_3. Thus, stem vapor bubbles form from the residual trapped vapor within the confined space, t_4. Because no active nucleation sites are required for stem bubble boiling, phase change occurs at reduced superheat compared to nucleate based boiling. This cycle then repeats.

the gap spacing threshold below which these stem bubbles form (*i.e.*, the transition from nucleation-suppressed to nucleation-active confined boiling). The formation of isolated spherical nucleated vapor bubbles is one of the distinct characteristics of nucleation-active confined boiling. On the other hand, significant viscous resistance induces the formation of the stem bubbles in nucleation-suppressed confined boiling. Therefore, one would expect that the confinement gap threshold is closely related to the vapor bubble growth dynamics near the heated surface. In general, the bubble growth process at any instant of time is affected by the interaction of the pressure difference across the two-phase interface and the fluid momentum, as well as by the rate of heat transfer across the two-phase interface. The contribution of each of these factors varies throughout the life cycle of the vapor bubble. Inertia-controlled growth dominates the hemispherical growth at early stages of bubble growth. During inertia-controlled growth, heat transfer to the interface is not the limiting factor, but rather the growth is limited by the momentum interaction between the bubble and the surrounding liquid. Once the vapor internal pressure equilibrates with surrounding liquid pressure, the bubble transforms into spherical shape and its growth rate is limited by relatively slower heat transfer rate across the two-phase interface [37], referred to as thermal-controlled growth. Hence, thermal-controlled growth exhibits lower viscous resistance compared to the inertia growth due to the difference in growth rate.

We propose that the rate of the vapor bubble growth directly correlates to the transition between nucleation-suppressed and nucleation-active confined boiling. We attribute the formation of stem bubbles to the variable liquid rewetting rate along the two-phase interface due to the significant viscous resistance. Because the viscous resistance of liquid flow is proportional to velocity, viscous resistance is expected to split the trapped bubble when the interface velocity is relatively high. The faster inertia-controlled bubble growth leads to higher viscous resistance compared to the thermal-controlled bubble growth. In addition, the trapped bubble could reach the confinement edge before equilibrating its internal vapor pressure to surrounding liquid pressure during the inertia-controlled growth. Furthermore, consequent stem bubbles would have radii of curvature smaller than the transition radius between inertia- controlled and thermal-controlled bubble growth, and hence, it would have high internal pressure which helps increasing the bubble ejection velocity from the confinement region. As a result, liquid replaces the escaped bubble volume at equally high velocity resulting in the formation of stem bubbles. In other words, vapor stem bubble enhancement mechanism is significant when the confinement gap is smaller than the transition radius from inertia-controlled to thermal-controlled growth. Van Stralen *et al.* [38] proposed that the temporal-dependence of the radius of the vapor bubble, $R(t)$, can be modelled as a superposition of the radii in the inertial-controlled, R_1, and the thermal controlled, R_2, regimes as:

$$R(t) = \frac{R_1(t)R_2(t)}{R_1(t) + R_2(t)}, \tag{3}$$

where R_1 and R_2 are defined as:

$$R_1 = 0.8165 \left(\frac{\rho_v h_{lv}(T_w - T_{sat}) exp\left(-\left(\frac{t}{t_d}\right)^{1/2}\right)}{\rho_l T_{sat}} \right) t, \tag{4}$$

$$R_2 = \left[1.9544\left(b^* exp\left(-\left(\frac{t}{t_d}\right)^{1/2}\right)\right) + 0.3730 Pr_l^{-1/6}\left(exp\left(-\left(\frac{t}{t_d}\right)^{1/2}\right)\right)\right] Ja(\alpha_l t)^{1/2}, \tag{5}$$

where ρ_l, α_l, and Pr_l are the density, thermal diffusivity, and Prandtl number of the liquid, h_{lv} is the latent heat of vaporization, $(T_w - T_{sat})$ is the superheat of the boiling surface, t is time, Ja is Jackob number, and t_d is the bubble departure time, which is obtained based on the departure diameter, d_d, using the following equations [39, 40]:

$$d_d = \sqrt{\frac{0.04^2 Ja^2 \sigma}{g(\rho_l - \rho_v)}}, \tag{6}$$

and

$$t_d = \frac{d_d}{0.59\left(\frac{\sigma(\rho_l - \rho_v)}{\rho_l^2}\right)^{1/4}}. \tag{7}$$

b^* is a geometrical correction factor to account for the fact that only portion of the hemispherical bubble near the heated surface is in contact with the superheated liquid. This parameter is defined as [38]:

$$b^* = 1.3908\frac{R_2(t_d)}{Ja\sqrt{\alpha t}} - 0.1908Pr_l^{-1/6}. \tag{8}$$

Figure 8 (a) the ratio of the heat transfer coefficient between confined and unconfined boiling ($h_{con}(q'')/h_{\infty}(q'')$) as a function of the heat flux for various gaps spacings. Figure 8 (a) illustrates the thermal enhancement magnitudes for various confined boiling spacings compared to similar heat flux levels in an unconfined cdnfiguration. Confinement enhances heat transfer at the lower range of heat fluxes tested while degrading heat transfer at the higher range of heat fluxes. Figure 8 (b) shows the temporal evolution of the non-dimensionalized diameter of the vapor bubble ($\Gamma = d/L$) using the above bubble growth model (Equations 3) for the range of superheats required for onset of nucleate boiling as observed during unconfined boiling testing ($T_i - T_{sat} \sim$ 4-5 °C). The criteria for onset of nucleation depend on the working fluid wettability and the surface morphology. Since the same boiling surface and working fluid are used in the unconfined tests, the nucleation onset superheat in unconfined boiling is used. During inertia-controlled growth, the bubble grows relatively fast and in a hemispherical shape. As the bubble growth transitions to the thermal-controlled growth, the bubble transforms into a spherical shape. In this study the transition between the two regimes is identified when the bubble growth rate decays by 90% of initial value. From Figure 8(b) we see this transition diameters, Γ, occur in the range of $\sim$ 0.35 - 0.5. Comparing to Figure 8(a), there is a noteworthy increase in the heat transfer enhancement when the confinement gap spacing, Bo, becomes smaller than this bubble transition diameters, Γ (note that both of these parameters are normalized by the same capillary length scale, so they can be directly compared in magnitude). This indicates that the transition in heat transfer enhancement mechanism from stem bubble boiling (nucleation-suppressed confined boiling) to microlayer based enhancement (nucleation-active confined boiling) occurs when the gap spacing is sufficiently small to obstruct the initial hemispherical vapor growth normal to the boiling surface.

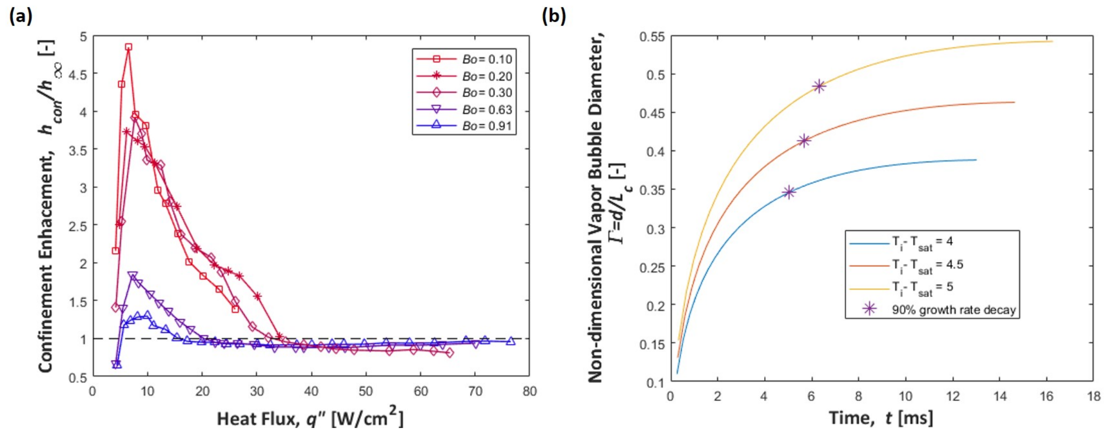

Figure 8: (a) Confinement enhancement ratio in the heat transfer coefficient compared to unconfined boiling ($h_{con}(q'')/h_{\infty}(q'')$) as a function of heat flux illustrating the impact of the gap size on the transition between nucleation-active to nucleation-suppressed confined boiling. (b) Temporal evolution of the non-dimensional vapor bubble diameter (d/L_c) predicted from Equations 3-8 for the range of heat fluxes required for the onset of nucleate boiling observed experimentally ($T_i - T_{sat} \sim$ 4-5 °C). The transition between inertia controlled and thermal controlled growth regimes occurs when the growth rate decays by 90% of initial value. Enhancements in heat transfer due to the vapor stem bubbles are significant when the confinement gap is smaller than the transition between the two bubble growth regimes.

4 Conclusions

In summary, we measure heat transfer characteristics and observe the interface dynamics for confined boiling of water occurring in confinement gap spacings from $Bo =$ 0.10 to 0.91. In agreement with earlier work on confined boiling, confinement enhances the heat transfer rate compared to unconfined boiling. However, previous work purported that the primary mechanism of enhancement was increased evaporation from a microlayer underneath the distorted vapor bubble, which cannot explain all past observations of enhancement in the past literature. Our work shows that the microlayer is indeed attributable for enhancement in heat transfer, but only for nucleation-active confined boiling ($0.5 \leq Bo \leq 1.0$). On the other hand, for nucleation-suppressed confined boiling ($Bo \leq 0.35$ - 0.5), newly observed vapor stem bubbles offer the dominant mechanism to enhance heat transfer. In this extremely confined regime, non-uniform surface rewetting result in only partial evacuation of the vapor exiting from the confinement gap. Thus, stem vapor bubbles form from the residual trapped vapor within the confined space. Because no active nucleation sites are required for stem bubble boiling, phase change occurs at reduced superheat compared to nucleate based boiling. This newly reported enhancement mechanism was observed both visually via a high-speed camera and is supported by the measured thermal response. Based on this improved understanding, three distinct confined boiling characteristics are identified (namely: nucleation-suppressed confined boiling, nucleation-active confined boiling, and partial dryout). Additionally, a threshold for the confinement gap spacing has been identified to predict the occurrence of stem bubble boiling. This improved understanding of the enhancement in heat transfer in extremely confined boiling has an important impact on designing compact two-phase thermal management solutions.

A Nucleation Onset Model

The incipience model used in Equation 2 is based on Hsu and Graham [28]. Starting from a mechanical force balance across the two-phase interface:

$$P_v = P_l + \frac{2\sigma}{r}, \tag{9}$$

where σ is the surface tension. Combining with the Clausius Clapyron equation,

$$\frac{\partial P}{\partial T} = \frac{T v_{fg}}{h_{fg}}, \tag{10}$$

and the conduction based temperature drop for the liquid near the boiling surface results in the following expression:

$$T_l = T_{sat} + \frac{T_{sat} v_{vf}}{h_{fg}} = T_w - \frac{q" a^* r}{k_l}, \tag{11}$$

where a^* is a geometrical factor that relates the height to the radius of the vapor embryo. In the confined configuration, a^* equals to 1 due to hydrodynamic deactivation. For the unconfined configuration, a^* equals to 1.6 [28] due to the ebullition cycle. Rearranging terms yields the following expression that can be solved for the active vapor embryo size:

$$\frac{q" a^* r^2}{k_l} - (T_w - T_{sat}) r + \frac{T_{sat} v_{fg} 2\sigma}{h_{fg}} = 0. \tag{12}$$

Specifically, the range of active vapor embryos sizes is given by

$$\left\{ \begin{matrix} r_{max} \\ r_{min} \end{matrix} \right\} = \frac{(T_w - T_{sat}) \left\{ \begin{matrix} + \\ - \end{matrix} \right\} \sqrt{(T_w - T_{sat})^2 - \frac{8q"}{k_l} \frac{\sigma T_{sat} v_{vg}}{h_{fg}}}}{2a^* \frac{q"}{k_l}}. \tag{13}$$

The onset condition corresponds to $r_{tan} = r_1 = r_2$, such that

$$r_{tan} = \frac{(T_w - T_{sat})}{2a^* \frac{q"}{k_l}}. \tag{14}$$

Plugging Equation 14 into Equation 12 yields the criteria for the heat flux at the onset of nucleate boiling:

$$q"_{onset} = \frac{h_{fg} k_l (T_w - T_{sat})^2}{8a^* \sigma T_{saT} v_f g}. \tag{15}$$

B Confinement Wall Size Effect

Both the normalized gap spacing above the boiling surface, Bo, and the confinement wall diameter, D_c, affect the thermal performance of confined boiling. Figure B.1 demonstrates the effect of extending the confinement wall lateral size above a fixed boiling surface diameter on heat transfer coefficient. The data indicates that extending the confinement wall diameter from 2.54 cm to 3.81 cm leads to an occurrence of partial dryout on the confined boiling surface and premature transition to nucleation-active boiling at a lower heat flux.

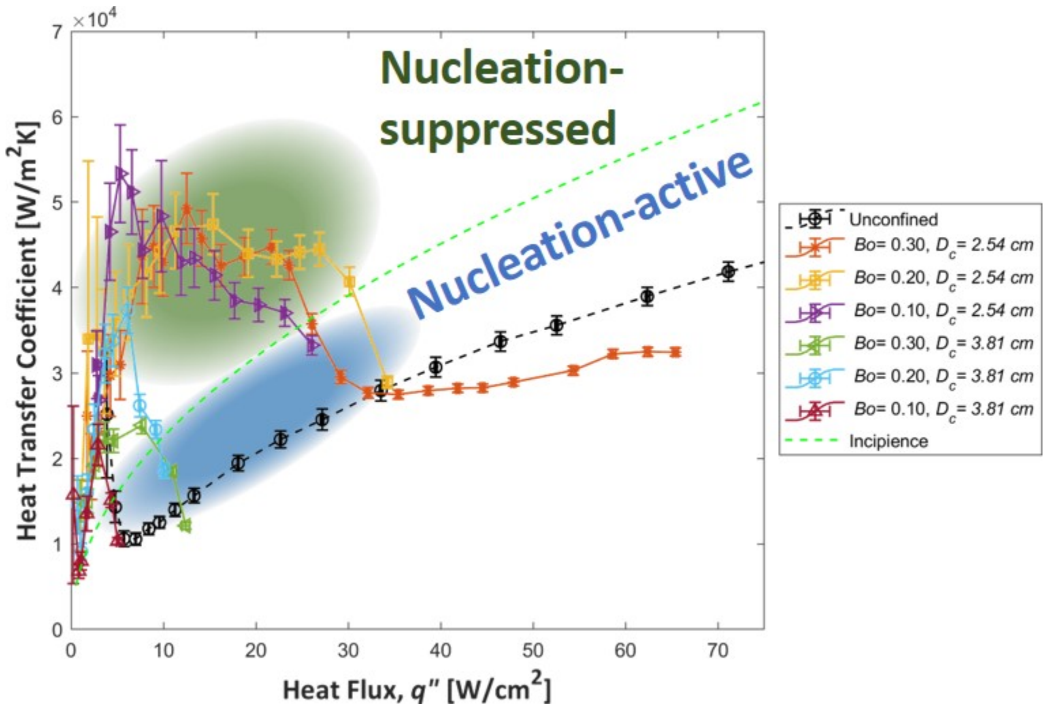

Figure B.1: The confinement wall size effect on the heat transfer coefficient of confined boiling. Extending the confinement wall diameter from 2.54 cm to 3.81 cm leads to an occurrence of partial dryout on the confined boiling surface and premature transition to nucleation-active boiling at a lower heat flux.

CRediT Authorship Contribution Statement

A. A. Alsaati: Conceptualization, Data Curation, Formal Analysis, Investigation, Methodology, Software, Validation, Visualization, Writing - original draft, and Writing - Review & Editing.

D. M. Warsinger: Project Administration, Resources, Supervision, and Writing - Review & Editing.

J. A. Weibel: Conceptualization, Funding Acquisition, Project Administration, Resources, Supervision, and Writing - Review & Editing.

A. M. Marconnet: Conceptualization, Funding Acquisition, Project Administration, Resources, Supervision, and Writing - Review & Editing.

Competing Interests

Authors have no competing interests to declare.

Acknowledgment

This work was supported by Semiconductor Research Corporation (SRC), as a part of the Global Research Collaboration (GRC) Program on Packaging (PKG; Science Director, Dr. John Oakley) in the Center for Heterogeneous Integration Research on Packaging (CHIRP). A.A. acknowledges the support of a Saudi Arabia Cultural Mission (SACM) fellowship, sponsored by the Saudi Arabian Ministry of Education. Some components of the pool boiling fixture were adapted from a system originally developed by Prof. Timothy Fisher and colleagues as reported in Ref. [34].

References

[1] I. Mudawar, "Assessment of High Heat Flux Thermal Management Schemes," *IEEE Transactions on Components, Packaging and Manufacturing Technology*, vol. 24, pp. 122–141, 2001.

[2] I. Mudawar, "Two-phase Microchannel Heat Sinks: Theory, Applications, and Limitations," *Journal of Electronic Packaging*, vol. 133, p. 041002, 2011.

[3] I. Mudawar, "Recent Advances in High-flux, Two-phase Thermal Management," *Journal of Thermal Science and Engineering Applications*, vol. 5, p. 021012, 2013.

[4] G. Liang and I. Mudawar, "Review of Spray Cooling Part 1: Single-phase and Nucleate Boiling Regimes, and Critical Heat Flux," *International Journal of Heat and Mass Transfer*, vol. 115, pp. 1174–1205, 2017.

[5] J. Broughton, V. Smet, R. R. Tummala, and Y. Joshi, "Review of Thermal Packaging Technologies for Automotive Power Electronics for Traction Purposes," *Journal of Electronics Packaging*, vol. 140(4), p. 040801, 2018.

[6] K. W. Jung, C. Zhang, T. Liu, M. Asheghi, and K. E. Goodson, "Thermal Management Research – from Power Electronics to Portables," in *IEEE Symposium on VLSI Technology*, (Honolulu, HI), 2018.

[7] D. Mallik, R. Mahajan, N. Raravikar, K. Radhakrishnan, K. Aygun, and B. Sankman, *Flip-Chip Packaging for Nanoscale Silicon Logic Devices: Challenges and Opportunities*. Springer, Cham, in: morris j. (eds) nanopackaging ed., 2018.

[8] J. A. Weibel and S. V. Garimella, "Recent Advances in Vapor Chamber Transport Characterization for High-Heat-Flux Application," *Advances in Heat Transfer*, vol. 45, pp. 209–301, 2013.

[9] A. Faghri, "Review and Advances in Heat Pipe Science and Technology," *Journal of Heat Transfer*, vol. 134(12), p. 123001, 2012.

[10] R. Chu, R. Simons, M. Ellsworth, R. Schmidt, and V. Cozzolino, "Review of Cooling Technologies for Computer Products," *IEEE Transactions on Device and Materials Reliability*, vol. 4, pp. 568–585, 2004.

[11] S. G. Kandlikar, "History, Advances, and Challenges in Liquid Flow and Flow Boiling Heat Transfer in Microchannels: A Critical Review," *Journal of Heat Transfer*, vol. 134, p. 034001, 2012.

[12] G. Klein and J. Westwater, "Heat Transfer from Multiple Spines to Boiling Liquids," *AIChE Journal*, vol. 17, pp. 1050–1056, 1971.

[13] R. Shimada, J. Komai, Y. Hirono, S. Kumagai, and T. Takeyama, "Enhancement of Boiling Heat Transfer in a Narrow Space Restricted by an Interference Plate with Holes," *Experimental Thermal and Fluid Science*, vol. 4, pp. 587–593, 1991.

[14] S. Liter and M. Kaviany, "Pool Boiling CHF Enhancement by Modulated Porous Layer Coating: Theory and Experiment," *Internatioanl Journal of Heat and Mass Transfer*, vol. 44, pp. 4287–4311, 2001.

[15] T. Harirchian and S. V. Garimella, "A Comprehensive Flow Regime Map for Microchannel Flow Boiling with Quantitative Transition Criteria," *International Journal of Heat and Mass Transfer*, vol. 53, pp. 2694–2702, 2010.

[16] S. G. Kandlikar, "Fundamental Issues Related to Flow Boiling in Minichannels and Microchannels," *Experimental Thermal and Fluid Science*, vol. 26, pp. 389–407, 2002.

[17] Z. LIU and R. H. S. WINTERTON, "A General Correlation for Saturated and Subcooled Flow Boiling in Tubes and Annuli, Based on a Nucleate Pool Boiling Equation," *International Journal of Heat and Mass Transfer*, vol. 34, pp. 2759–2766, 1991.

[18] P. A. Kew and K. Cornwell, "Correlations for the Prediction of Boiling Heat Transfer in Small Diameter Channels," *Applied Thermal Engineering*, vol. 17, pp. 705–715, 1997.

[19] Y. Katto and S. Yokoya, "Experimental Study of Nucleate Pool Boiling in Case of Making Interference-plate Approach to the Heating Surface," in *Proceedings of*

3rd International Journal of Heat Transfer Conference, (Chicago, USA), pp. 219–227, 1966.

[20] Y. Katto, S. Yokoya, and K. Terakoa, “Nucleate and Transition Boiling in a Narrow Space Between Two Horizontal Parallel Disk Surfaces,” *Bulletin of JSME*, vol. 20, pp. 638–643, 1977.

[21] M.Kapitz, F. Reinker, and S. aus der Wiesche, “Viscous Fingering and Heat Transfer During Boiling in a Hele–Shaw Cell,” *Experimental Thermal and Fluid Science*, vol. 67, pp. 18–23, 2015.

[22] M. Misale, G. Guglielmini, A. Priarone, and C. Ambientale, “HFE-7100 Pool Boiling Heat Transfer and Critical Heat Flux in Inclined Narrow Spaces,” *International Journal of Refrigeration*, vol. 32, pp. 235–245, 2009.

[23] M. Misale, G. Guglielmini, and A. Priarone, “Nucleate Boiling and Critical Heat Flux of HFE-7100 in Horizontal Narrow Spaces,” *Experimental Thermal and Fluid Science*, vol. 35, pp. 772–779, 2011.

[24] R. R. Souza, J. C. Passos, and E. M. Cardoso, “Confined and Unconfined Nucleate Boiling under Terrestrial and Microgravity Conditions,” *Applied Thermal Engineering*, vol. 51, pp. 1290–1296, 2013.

[25] M.Kapitz, L. Schmiedinghoff, S. J. Lüling, and S. aus der Wiesche, “Impact of Surface Parameters on Confined Boiling Heat Transfer in a Hele-Shaw Cell,” *Heat and Mass Transfer*, vol. 55, pp. 2533–02604, 2019.

[26] A. Sarode, R. Raj, and A. Bhargav, “On the Role of Confinement Plate Wettability on Pool Boiling Heat Transfer,” *international Journal of Heat and mass Transfer*, vol. 156, p. 119723, 2020.

[27] M.G.Cooper and A.J.P.Lloyd, “The Microlayer in Nucleate Pool Boiling,” *International Journal of Heat and Mass Transfer*, vol. 12, pp. 895–913, 1969.

[28] Y. Y. Hsu and R. W. Graham, “An Analytical and Experimental Study of the Thermal Boundary Layer and Ebullition cycle in Nucleation Boiling,” *NASA*, vol. TN-D-594, 1961.

[29] B. Stutz, M. Lallemand, F. Raimbault, and J. Passos, “Nucleate and Transition Boiling in Narrow Horizontal Spaces,” *Heat and Mass Transfer*, vol. 45, pp. 929–935, 2009.

[30] M. Lallemand, J. Bonjour, D. Gentile, and F. Boulanger, “The Physical Mechanisms Involved in the Boiling of Mixtures in Narrow Spaces,” in *International Heat Transfer Conference*, (Kyongjiu, Korea), pp. 515–519, 1998.

[31] R. R. Souza, E. M. Cardoso, and J. Passos, “Confined and Unconfined Nucleate Boiling of HFE7100 in the Presence of Nanostructured Surfaces,” *Experimental Thermal and Fluid Science*, vol. 91, pp. 312–319, 2017.

[32] E. Cardoso, O. Kannengieser, B. Stutz, and J. C. Passos, “FC72 and FC87 Nucleate Boiling Inside a Narrow Horizontal Space,” *Experimental Thermal and Fluid Science*, vol. 35, pp. 1038–1045, 2011.

[33] A. Alsaati, J. A. Weibel, and A. Marconnet, “Confined Immersion Cooling in Microscale Gaps,” in *2020 19th IEEE Intersociety Conference on Thermal and Thermomechanical Phenomena in Electronic Systems (ITherm)*, (Orlando, FL, USA), 2020.

[34] C. N. Hunter, N. R. Glavin, C. Muratore, T. S. Fisher, J. G. Jones, S. A. Putnam, A. N. Khramov, and C. H. Li, “Micro-patterned substrates with nanoscale elements for pool boiling,” in *ASME/JSME 8th Thermal Engineering Joint Conference*, (Honolulu, Hawaii, USA), 2011.

[35] J. H. Linehard and V. K. Dhir, “Extended Hydrodynamic Theory of The Peak and Minimum Pool Boiling Heat Fluxes,” *NASA CR-2270*, 1973.

[36] Y. Y. Hsu, “On the Size Range of Active Nucleation Cavities on a Heating Surface,” *ASME. Journal of Heat Transfer*, vol. 84, pp. 207–213, 1962.

[37] V. P. Carey, *Liquid-Vapor Phase-Change Phenomena.* New York, NY: Taylor and Francis, second ed., 2008.

[38] S. J. D. V. Stralen, M. S. Sohal, R. Cole, and W. M. Sluyter, “Bubble Growth Rate in Pure and Binary Systems: Combined Effect of Relaxation and Evaporation Microlayer,” *International Journal of Heat and mass Transfer*, vol. 18, pp. 453–467, 1975.

[39] R. Cole, “Bubble Frequencies and Departure Volumes at subatmospheric Pressures,” *AIChE Journal*, vol. 13, pp. 779–783, 1967.

[40] N. Zuber, “Nucleate Boiling - The Region of Isolated Bubbles - Similarity with Natural Convection,” *International Journal of Heat and mass Transfer*, vol. 6, pp. 53–65, 1963.